Research Square

Preprints are preliminary reports that have not undergone peer review.
They should not be considered conclusive, used to inform clinical practice,
or referenced by the media as validated information.

Mid-field MRI with cochlear implants: A healthy volunteer study of magnet displacement, pressure perception, and temporal bone imaging

Steve E.J. Connor
steve.connor@kcl.ac.uk

King's College London
Anthony Price
King's College London
Irumee Pai
Guy's and St Thomas' NHS Foundation Trust
Philip Touska
Guy's and St Thomas' NHS Foundation Trust
Cristina Dudau
King's College Hospital NHS Foundation Trust
Philippa Bridgen
King's College London
Pierluigi Cio
King's College London
Lucy Billimoria
King's College London
Daniel West
Guy's and St Thomas' NHS Foundation Trust
Oscar Lally
Guy's and St Thomas' NHS Foundation Trust
Sebastien Ourselin
King's College London
Joseph V Hajnal
King's College London

Research Article

Keywords: Cochlear Implants, Magnetic Resonance Imaging, Equipment Safety, image artefacts, temporal bone imaging, low-field MRI

Posted Date: August 14th, 2026

DOI: https://doi.org/10.21203/rs.3.rs-10550261/v1

License: This work is licensed under a Creative Commons Attribution 4.0 International License. Read Full License

Additional Declarations: No competing interests reported.

Abstract

Purpose

We hypothesised that 0.55T MRI would reduce magnet displacement risk and pressure perception compared to 1.5T MRI in healthy volunteers with bandaged cochlear implants (CIs) containing axial or rotating diametric magnets, while maintaining temporal bone image interpretability.

Methods

Ten healthy volunteers were bandaged with CIs (5 axial magnet; 5 rotating diametric magnet) and underwent consecutive 0.55T and 1.5T MRI sessions. Pressure perception was assessed using a visual analogue scale and magnet displacement was evaluated. Optimised 2D T2-weighted fast spin echo (2D T2-FSE) and constructive interference in steady state (CISS) temporal bone sequences were acquired at both field strengths in seven participants. Diagnostic confidence, artefactual degradation, and distances from CI-related artefact to anatomical structures were assessed. CI magnet translational and torque force were measured. Paired ordinal data were analysed using Wilcoxon signed-rank and Bland–Altman analysed agreement of distances.

Results

Axial CI magnets were displaced after 1.5T MRI in 4/5 participants but not 0.55T ($p = 0.04$) with corresponding torque measured as 0.133 v 0.062 Nm. Rotating diametric magnets showed no displacement at either 1.5T or 0.55T with similar torque measurements at both field strengths (0.046 v 0.044 Nm). Pressure perception did not differ between MRI systems. Both CISS and 2D T2-FSE sequences provided adequate diagnostic confidence at both field strengths. The 0.55T 2D T2-FSE sequence reduced CI-related artefact and allowed similar diagnostic confidence to 1.5T. Distances between artefact and anatomical structures did not differ between scanners.

Conclusion

Mid-field 0.55T MRI reduced axial CI magnet displacement while maintaining clinically acceptable temporal bone imaging. It may provide a useful addition to CI imaging in patients with axial magnet CIs who have experienced magnet complications or pain when undergoing high field MRI.

Introduction

Over 1.5 billion individuals experience significant disability from hearing loss [1], and there are now more than one million cochlear implant (CI) recipients worldwide [2]. Alongside this, increasing availability, life expectancy, and expanding clinical indications have driven rising magnetic resonance imaging (MRI) utilisation. There are 40.6–122.8 examinations performed annually per 1,000 population across developed economies [3], predominantly using 1.5T systems [4]. Consequently, the number of CI recipients undergoing MRI continues to grow, and most are expected to require MRI during their lifetime [5].

The internal magnet and metal lic components of a cochlear implant (CI) interact with the static magnetic field (B_0), gradient fields, and radiofrequency fields during MRI. This gives rise to important safety considerations, including translational forces, torque, heating, image artefact and demagnetisation which limit MRI in CI recipients. Imaging at lower field strength with a 0.55T mid-field MRI system (MAGNETOM Free.Max, Siemens Healthineers) may mitigate some of these effects by reducing induced forces, heating, and artefact.

A major source of adverse events is magnet-related translational force and torque within the static magnetic field. This can cause significant patient discomfort leading to premature termination of MRI [6–9], while magnet displacement may impair device function or require explantation. Traditional axial CI magnets, with a fixed pole oriented toward the skin flap, are especially susceptible to torque perpendicular to the skull, resulting in axial rotation even with head bandaging. Newer designs incorporating self-aligning diametric magnets or screw-fixation mechanisms reduce this torque and associated complications [10–16]. Despite these advances, MRI-related adverse events remain increasingly reported, likely reflecting both the persistence of legacy axial magnet designs and the rising use of MRI [10]. As torque is proportional to B_0, assuming the internal magnetisation remains constant, it is expected to decrease at lower field strengths [17]. However, the effect of lower field MRI on patient tolerance and magnet displacement risk, particularly across different magnet designs, remains to be established.

A further key constraint is RF exposure, typically expressed as specific absorption rate (SAR), which must be limited in accordance with manufacturer-defined MRI-conditional guidelines to minimise device heating [18]. At lower field strengths, RF energy deposition is both reduced (scaling with B_0^2) and more homogeneous [19] which improves safety margins and facilitates compliance with MRI-conditional limits. This may allow greater flexibility in sequence design while maintaining safer operating conditions for CI patients. These benefits must be balanced against reduced signal-to-noise ratio (SNR), which can affect spatial resolution and increase scan time. However, with modern hardware and software, lower-field MRI has been shown to provide comparable diagnostic confidence to 1.5T for temporal bone imaging [20].

Finally, the highly non-linear magnetic field generated by the internal CI magnet produces substantial artefact, including signal loss from intravoxel dephasing, geometric distortion of the slice-select profile, and in-plane distortion with signal pile-up and dropout. The extent of artefact is influenced by implantation site [21], head position [22, 23], and sequence [11, 21, 23–28]. Signal loss from CI magnets rapidly saturates at clinically relevant echo times and bandwidths, so it remains uncertain whether lower field strengths provide a meaningful reduction in artefact.

It was hypothesised that mid-field 0.55T MRI would 1) result in a lower risk of CI magnet displacement and 2) there would be maintained image quality and similar impact of CI-related artefact compared with high-field 1.5T MRI. This was explored using healthy volunteers with CI bandaged in place as a surrogate system.

Methods

Cochlear implant magnet translational force and torque testing

The translational force and torque were tested for the two non-functioning MRI-conditional Advanced Bionics CIs (Advanced Bionics, Stäfa, Switzerland) used in this healthy volunteer study. These were a HiRes™ Ultra 3D CI with a self-aligning diametric magnet, and a HiRes 90K™ CI with an axial magnet.

The translational force experienced by each of the cochlear implants was estimated using the deflection angle method described by ASTM F2052-21 standard [29]. Each implant was suspended by lightweight super-strong thread (30D gel spun polyethylene) after securing the implant magnet with tape within its silicone housing. The device was advanced along the central z-axis (x=y=0) of the scanner to establish the point of maximum deflection. Due to the significant increase in field gradient on the 1.5T system, additional weights (15g) were attached to reduce the angle to a desirable range. The spatial magnetic field was subsequently measured at increments along the same line using a 3-axis Hall probe (Metrolab ETM-1). Knowing the mass of each device (plus weights) provided estimates of the force experienced on entering the scanners. It was assumed that the magnet was permanently saturated at both field strengths and the force on the titanium casing was negligible, thus the expectation was that the force was proportional to the spatial gradient of the magnetic field only.

The torque experienced by each device was measured at the isocentre of both scanners using a custom-made torsion spring rig according to the ASTM F2213-17 standard [30]. Due to the large forces expected on the cochlear implant magnet at the centre of the scanner, the silicone housing was first splinted between a rigid plastic bracket and cover plate, before mounting on the torque rig with the centre of the magnet aligned along the axis of the rig pivot point. The rig was fitted with SPEC® torsion springs of constant k=0.1107 Nm/rad. Each device was rotated through 360° at 10° increments with the deflection angle recorded to determine the maximum deflection and thus torque. The process was repeated twice and recorded by two observers for each device at both 0.55 and 1.5T.

Participants

The study was approved by the institutional Health Faculties (Purple) Research Ethics Subcommittee (Reference: HR/DP-23/24-40213). The research was conducted in accordance with the Declaration of Helsinki. Healthy volunteers were recruited between June 2024 and June 2025. Written informed consent was obtained from all participants in this study.

Exclusion criteria included known temporal bone abnormalities, auditory implants, facial pain or headache disorders, MRI contraindications, and prior knowledge of the MRI scanner locations within the unit. The institutional MRI safety and technical assurance committee performed a risk assessment since the previous MRI conditional testing only applied to 1.5T scanning and to implanted patients.

CI bandaging

A non-functioning MRI-conditional CI was bandaged to the head of each participant by an experienced clinician. The first five participants received a HiRes™ Ultra 3D CI with a self-aligning diametric magnet, and the subsequent five a HiRes 90K™ CI with an axial magnet. The magnet housing was reinforced with felt padding applied to the undersurface and a hard plastic disc taped to the superficial aspect (Fig 1). Bandaging tension was standardised by using a single full head wrapping of the bandage with an unstretched length of 80% of head circumference. CIs were positioned at varying angles [26] relative to the nasion–external auditory meatus (EAM) plane using a digital protractor (Fig 1, Table 1). A dummy processor was applied to aid anatomical positioning relative to the pinna, and the CI–EAM distance was recorded. Rebandaging was performed between scan sessions in six participants in order to evaluate for CI magnet displacement.

MRI scanning

Each participant underwent consecutive one-hour MRI sessions on 0.55T (Siemens MAGNETOM Free.Max) and 1.5T (Siemens MAGNETOM Sola) scanners, with scan order randomly assigned in a balanced fashion. Scanner signage was masked to maintain participant blinding to field strength. Participants were positioned with the head kept neutral and with flexion matched between scanners. They were lowered gently onto the couch, avoiding proximity to the magnet bore edge. MRI sequences varied between sessions and included both whole-brain and dedicated temporal bone protocols.

Pressure sensation scoring and magnet displacement

Pressure sensation at the site of the bandaged CI was assessed using a visual analogue scale (VAS) adapted to a 10-point ordinal scale ranging from no pressure to marked pressure and discomfort (Supplementary Fig 1) [7,16,31]. The scale was explained to participants prior to bandaging, and they were instructed to report the maximum pressure experienced, localised to the CI site. Baseline scores were obtained 3-4 minutes after bandaging, and prior to each of the two scans. Within the MRI environment, pressure was recorded immediately upon entering the bore, where closest to the region of maximal translational force, and participants were also asked about any sensation of clicking. A second assessment was performed immediately after the scanning to reflect the period when at the isocentre and conditions of maximal torque. Participants were additionally asked whether any changes in sensation were transient or sustained.

CI magnet position within the silicone housing was assessed after completion of both scan sessions in all participants, and additionally after the first session in five participants with the HiRes™ 90K CI and one participant with the HiRes™ Ultra 3D CI prior to rebandaging in an identical CI position. Displacement was classified as tilting when the magnet did not cross the housing lip, and dislocation when it did (Fig 2, Table 2).

Sequence development /parameters

Dedicated T2-weighted temporal bone MRI sequences were developed to minimise CI-related artefact while optimising visualisation of structures within the cerebellopontine angle cisterns (CPAs), internal auditory meati (IAMs), and inner ears. Two-dimensional T2-weighted fast spin echo (2D T2-FSE) and three-dimensional constructive interference in steady state (CISS) sequences were adapted within specific absorption rate (SAR) limits for MRI-conditional CIs (Supplementary Table 1). The conditional MRI limits for 1.5T were also applied to 0.55T MRI scanning. Optimisation differed between scanners due to lower SNR at 0.55T and higher SAR for the same drive conditions at 1.5T.

Multiple strategies were used to reduce CI-related obscuration of the temporal bone. Receiver bandwidth was increased while maintaining acceptable SNR, and the frequency encoding direction was chosen to shift off-resonance artefact away from the temporal bones. Voxel size was reduced on 2D T2-FSE to improve spatial resolution and reduce susceptibility effects. A higher slice selection bandwidth did not clearly benefit and was not applied. The reduction in SNR due to the decreased field strength and increased receiver bandwidth at 0.55T was compensated by increasing the number of signal averages and applying AI-based reconstruction. At 1.5 T, SAR constraints (Supplementary Table 1) limited sequence flexibility for the HiRes 90K™ cochlear implant and required iterative optimisation of imaging parameters, including reduced flip angle and increased repetition time (TR), to maintain compliance with manufacturer-specified MRI conditions.

Following optimisation, study protocol temporal bone sequences were acquired in 3 participants with the HiRes™ Ultra 3D CI and 4 participants with the HiRes 90K™ CI (Supplementary table 2).

Image analysis

The individual CISS and 2D T2-FSE sequences acquired at 0.55T and 1.5T for the seven participants were organised into 28 folders and randomly reordered. Image analysis was performed using Horos (v4.0.1; The Horos Project, Annapolis, MD, USA) [32] with consistent windowing. The 3D multiplanar reformat module was used to obtain standardised angulation of the image plane for all sequences with a thin reconstruction increment. Quantitative and qualitative assessments were undertaken using built-in tools. Three radiologists (PT: 9 years; SC: 27 years; CD: 14 years' head and neck subspecialty experience) independently reviewed the images following a training session on non-study cases to ensure consistency.

A 5-point ordinal scale was used for all evaluations. Image quality remote from CI artefact was assessed first, followed by diagnostic confidence and CI-related artefact at the CPA (1 cm on either side of the porus acousticus), IAM, and inner ear on both the implanted and contralateral sides (Table 3, Figure 3). Diagnostic confidence reflected visualisation of cranial nerves and fluid spaces, incorporating both image quality and artefact effects. CI-related artefact was graded according to the degree of structural obscuration. Artefact type was also recorded as signal drop-out, signal pile-up, banding, spatial distortion, or warping.

Given variable slab coverage, minimum in-plane distances were measured between artefact and relevant anatomical markers. This provided a consistent planar proximity metric rather than a global 3D minimum but avoided bias when regions of maximal artefact fell outside the acquired volume. The border of the hard artefact was defined as signal void or pileup where there was no visualisation of the expected signal due to underlying anatomical structures. Measurements were taken from the hard artefact to the posterior lip of the porus acousticus at the axial level of the vestibulocochlear nerve, and to the cochlear aperture bilaterally (Figure 4). On the ipsilateral side, additional measurements were obtained in orthogonal coronal or sagittal planes. It was noted when the contour of the hard artefact indicated that the nearest margin lay outside the craniocaudal field of view and these cases were excluded from analysis (Figure 4).

A second scoring session, performed two weeks later to reduce recall bias, directly compared equivalent 0.55T and 1.5T sequences for image quality, diagnostic confidence, and CI-related artefact (Table 3).

Statistical analysis

Statistical analyses were performed using SPSS (v27.0; IBM, USA), with $p < 0.05$ considered statistically significant.

Paired ordinal data (pressure sensation, magnet displacement, diagnostic quality, diagnostic confidence, and CI artefact scores) were compared using the Wilcoxon signed-rank test (exact, two-tailed).

Comparisons were performed between CISS and T2-FSE sequences at each field strength and between 0.55T and 1.5T for each sequence. Effect size was calculated as $r = Z/\sqrt{n}$, and the number of superior rankings was recorded. A secondary direct comparison of equivalent 0.55T and 1.5T sequences was undertaken as a sensitivity analysis against the blinded ranking results.

Bland–Altman analysis assessed agreement between sequences and field strengths for measured CI artefact distances to adjacent anatomical structures, with mean bias, 95% limits of agreement, and confidence intervals for the limits reported.

Inter-observer reliability for ordinal and continuous variables was assessed using intraclass correlation coefficients (ICC; two-way random-effects, absolute agreement, single measures).

Results

Cochlear implant magnet translational and torque force testing

The translational force on each implant due to magnetically induced deflection was estimated for both 0.55 and 1.5T scanners. The maximum angle observed for both implants on each scanner was close to the bore entrance, which correlated with the expected point of maximum spatial field gradient along the central z-axis. The calculated translational forces on the HiRes™ Ultra 3D and HiRes™ 90K CIs were 0.13 and 0.09N approaching the 0.55T system, and 0.41 and 0.31N, approaching the 1.5T system. This increase in force approximately scales with the increase in measured maximum spatial field gradient between the two system at ~0.88T/m vs 2.7T/m for the 0.55 and 1.5T systems, respectively.

The average maximum measured torque on the HiRes™ Ultra 3D CI revealed a lower and relatively field-independent relationship with values of 0.046 Nm and 0.044 Nm at 0.55 and 1.5T. Conversely, the HiRes™ 90K CI exhibited a higher maximum torque of 0.061 Nm and 0.133 Nm at 0.55 and 1.5T. The significantly higher torque measured with the HiRes™ 90K CI at 1.5T also translated to a large force given the smaller diameter of the internal magnet (9mm for HiRes™ 90K vs 12mm for the HiRes™ Ultra 3D). Ultimately, this led to an estimated maximum force of of 7.73N and 7.25N for the HiRes™ Ultra 3D with corresponding values of 3.7N at 0.55T and 29.6N at 1.5T for the HiRes™ 90K CI.

Participants and CI magnet position

Ten participants were enrolled (6 men, 4 women; median age 37 years, IQR 19). Four CIs were bandaged at a baseline nasion–EAM angle of 120°, with the remaining six positioned at equal positive and negative increments and at 8–10 cm from the EAM (Table 1). The order of 0.55T and 1.5T scanning was balanced across participants.

Pressure sensation and magnet displacement

Pressure scores on the VAS are shown in Table 2. Baseline scores were similar between scanners (0.55T: median 1 [IQR 0–1.5]; 1.5T: median 1 [IQR 0–1]). On entering the scanner bore, median change in pressure was 0 [IQR 0–0] for both 0.55T and 1.5T, with no significant difference between field strengths (Wilcoxon signed-rank test, $Z = -0.378$, exact $p = 0.71$). During scanning, median pressure scores were 1 [IQR 0–2] at 0.55T and 2 [IQR 0–3] at 1.5T, again with no significant difference ($Z = -0.105$, exact $p = 0.92$). In addition, no significant difference in pressure score changes were observed when analysing the two CI models separately.

There were no magnet displacements in the HiRes™ Ultra 3D CI at either field strength (0/5). In contrast, 4/5 HiRes™ 90K CI magnets showed displacement within the silicone housing after 1.5 T imaging with 2 tilted and 2 dislocated, whereas there was no displacement at 0.55T (Table 2, Figure 2). This represented a significantly higher incidence of HiRes 90K™ magnet displacement at 1.5T compared with 0.55T (Wilcoxon signed-rank test, $Z = -2.00$, exact $p = 0.04$).

Qualitative image analysis

Image quality and diagnostic confidence for ipsilateral anatomical structures showed no significant differences in median scores between sequences or field strengths ($p > 0.05$; Table 4). However, superior rankings and a large effect size ($r > 0.5$) suggested improved image quality with CISS at 1.5T compared with 0.55T, translating into higher diagnostic confidence at both the ipsilateral and contralateral CPAs ($r = 0.63$; $r=0.51$) and IAMs ($r = 0.80$; $r=0.80$). The 2D T2-FSE sequence demonstrated higher diagnostic confidence scores than CISS for ipsilateral inner ear imaging at both 0.55T ($r = 0.78$) and 1.5T ($r = 0.58$), likely reflecting degradation from CISS banding artefact. Of the 28 sequence assessments (4 sequences in 7 participants), low diagnostic confidence at the ipsilateral CPA was recorded in only 3 cases, all at 0.55T. No cases of low diagnostic confidence were observed at either field strength for the IAM or inner ear, with high or very high diagnostic confidence being reported in 20/28 assessments.

No significant differences were observed between 0.55T and 1.5T in qualitative visualisation without CI-related artefact at any ipsilateral anatomical site ($p > 0.05$; $r < 0.5$; Table 4). 2D T2-FSE demonstrated better visualisation than CISS at both field strengths ($r > 0.5$), reaching statistical significance at 0.55T ($p < 0.05$). Complete or near-complete visualisation was achieved in 24/28 CPA, 26/28 IAM, and 20/28 inner ear assessments. All 2D T2-FSE sequences demonstrated complete visualisation of all structures except for one inner ear case at 0.55T.

On the contralateral side, all anatomical structures were fully visualised with both sequences and field strengths, and no low diagnostic confidence scores were recorded. Non-significant superior diagnostic confidence scores were again observed at 1.5T compared with 0.55T, more evident with CISS at the IAM and inner ear. The improved diagnostic confidence scores of 2D T2-FSE were less pronounced contralaterally, with CISS performing better at the CPA ($r = 0.51$ at 0.55T; $r = 0.65$ at 1.5T), despite greater CI artefact burden.

Sensitivity analysis using direct 0.55T versus 1.5T sequence comparisons confirmed the same direction of effect, with higher scores where large effect sizes were identified in the primary analysis and no contradictory trends.

Interobserver agreement ranged from moderate to excellent (ICC 0.52–0.92; Table 4). Types of artefacts contributing to image degradation are summarised in Supplementary Table 3

Quantitative image analysis

Hard artefact was present on the target image allowing measurement to anatomical structures in 30/42 for 2D T2-FSE at 0.55T, 28/42 at 1.5T, 38/42 for CISS at 0.55T, and 42/42 at 1.5T. Two additional coronal 2D T2-FSE measurements at both field strengths were excluded by consensus, since the closest artefact

margin lay outside the field of view.

Bland–Altman analysis demonstrated small mean differences when comparing CISS with 2D T2-FSE at both field strengths, and when comparing 0.55T with 1.5T for each sequence (Tables 5-6, Figure 5, Supplementary Figure 2). Most measurements showed only slightly greater distances (10/12 being <1 cm) between artefact and adjacent structures on 2D T2-FSE compared with CISS at both 0.55T and 1.5T. Across the measurements, there was a tendency towards larger distances on 0.55T imaging with the CISS sequence and for larger distances at 1.5T for the 2D T2-FSE sequence. However, there was wide variability in the hierarchy of distances between participants as depicted in figure 5 for the ipsilateral porus acousticus measurement. The confidence intervals for the limits of agreement included zero for all comparisons, indicating no clear systematic bias, although estimates were imprecise due to small sample size. No proportional bias was identified on linear regression of difference versus mean.

Interobserver agreement for quantitative measurements was excellent, with ICCs of 0.91 (0.82–0.96) and 0.89 (0.80–0.95) for axial ipsilateral, 0.91 (0.82–0.96) and 0.92 (0.85–0.96) for coronal ipsilateral, and 0.91 (0.82–0.96) and 0.92 (0.85–0.96) for contralateral axial measurements.

Discussion

An axial cochlear implant (CI) magnet was displaced after 1.5 T MRI in 4/5 participants but was never displaced after 0.55 T MRI (P = 0.04). In contrast, a CI incorporating a rotating diamagnetic magnet showed no displacement at either field strength. These findings were explained by differences in measured torque and translational forces. Whereas the diamagnetic CI magnet demonstrated similar maximum torque values at 0.55 and 1.5T, the axial CI magnet torque estimates showed higher values and a ~ 2.2-fold increase at 1.5T compared to 0.55T. Participant-reported pressure scores on entering the scanner bore (p = 0.71) or during scanning (p = 0.92) did not differ significantly between the 0.55T and 1.5T MRI systems. 2D T2-weighted fast spin echo (2D T2-FSE) and three-dimensional constructive interference in steady state (CISS) temporal bone sequences, optimised for imaging in the presence of CI-related artefact, provided at least adequate diagnostic confidence for evaluating relevant anatomical structures in almost all cases at both field strengths. The 0.55T MRI achieved comparable diagnostic confidence to 1.5T with the 2D T2-FSE sequence and, unlike at 1.5T, the SAR limits were not exceeded for the axial magnet CI. The quantitative measures evaluating proximity of CI-related hard artefact to temporal bone structures did not clearly differ between 0.55T and 1.5T, although estimates were limited by small sample size.

Magnet displacement was the most frequently reported device malfunction [10, 33] in the era prior to rotatable diametric magnets. Whilst rates of up to 9.1% were recorded in retrospective series [6,8,13,34,35], prospective cohorts of CI patients with axial magnets have demonstrated it to be less frequent at 0-4.4% [7, 9, 12, 14, 36]. Our finding of very high rates (80%) of magnet tilting with the HiRes 90K™ CI may reflect less containment of the magnet by the bandaging in our healthy volunteers compared to that offered by the scalp flap in CI recipients. In addition, our direct examination of the magnet within the housing [37] may have provided greater sensitivity to the detection of clinically occult minor magnet tilting. The newer devices with diametric magnets are considered to have eliminated the risk of magnet displacement at high field MRI [10–13, 15, 16, 33, 38] and this was supported by our findings of no HiRes™ Ultra 3D magnet displacements at either 0.55T or 1.5T.

The torque exceeded the translational force and increased with field strength as expected for the axial magnet CI, whereas the diametric magnet CI remained relatively constant between field strengths. The torque measurements for the HiRes™ Ultra 3D at 1.5T were closely aligned to previously reported values [27]. Tysome et al also measured torque for the same HiRes 90K™ CI at 1.5T, reporting a higher maximum value of 0.186Nm, four times higher the HiRes™ Ultra 3D magnet. Our slightly lower values for the axial magnet could be partly due to the difficulty in securely clamping the small internal magnet, potential malalignment with the pivot point of the rig or partial demagnetisation of the magnet from previous scanning. A single report comparing torque of an axial (Clarion 1.2) magnet at 1.5T with 0.3T also demonstrated decreased torque at lower field MRI (0.19 v 0.04Nm) [39].

Despite differences in rates of magnet displacement between MRI systems and cochlear implant models, this did not translate into corresponding changes in pressure scores in this sham study. Pain is the most common adverse clinical manifestation in patients with cochlear implants undergoing MRI and is thought to predominantly result from torque causing movement of the magnet within the static magnetic field. It has been reported to result in premature termination of MRI examinations in up to 28% of patients with axial magnets [8, 12, 38, 40] whilst this is uncommon in patients with self-aligning diametric magnet CIs [11, 12, 14, 9, 36, 40]. Patel et al. demonstrated reduced pain scores in a prospective comparison of patients with axial versus self-aligning diametric magnets undergoing MRI [14]. In the present study, the absence of a clear differences in pressure scores between CI magnets or MRI systems may reflect both the small sample size, the cushioning effect of scalp and hair and the influence of confounding factors. Although mitigation strategies were employed, subtle variations in bandage tightness, differences in local pressure from padding over the protruding implant assembly, and psychological factors may have varied between scan sessions and participants. While severe pain is often associated with magnet displacement [6, 34, 36], it is also plausible that the pressure sensations reported in our cohort were driven more by external compression from bandaging than by the minor magnet movement [12, 36]. It is also of note that studies examining pressure–pain thresholds in the temporal region have demonstrated substantial inter-individual variability [41], a finding that is mirrored in reports of CI patients undergoing MRI [6, 7, 12].

Whilst the evolution of CIs with diametric magnets has markedly improved the MRI safety profile of CIs, patients with older models continue to require MRI. The number of CI-related medical device reports submitted to the Food and Drug Administration (FDA) has remained at 56–142 per year since 2019, a period in which all three major CI manufacturers have offered devices with diametric rotatable magnets [33]. Some patients undergoing serial MRI studies may experience adverse events due to magnet displacement at high field MRI such that magnet removal is considered. The absence of any magnet displacement at 0.55T with the axial magnet CI, supported by objective measures of reduced torque and longitudinal displacement suggests that imaging such patients with older CI models at mid-field [42] may represent an alternative pathway to mitigate this risk.

MRI of the temporal bone may be required in the post CI patient for monitoring vestibular schwannomas, for investigation of new audio-vestibular symptoms, and for MRI-based evaluation of cochlear implant electrode arrays [43]. Before recommending mid-field temporal bone MRI in cochlear implant recipients, it

is important to ensure that the reduced signal-to-noise ratio and sequence modifications required to limit CI-related artefact, do not compromise the imaging. A newer generation of lower field MRI systems benefit from being equipped with the latest hardware and software from high-field technology and artificial intelligence-based reconstruction [20]. Our qualitative analysis demonstrated that 0.55T imaging provides sufficient diagnostic quality for assessment of the CPA, IAM and inner ear. Whilst CISS generally resulted in greater obscuration of anatomical structures than 2D TSE/FSE due to associated banding artefact, the two sequences may be complementary at 0.55T. The 0.55T 2D TSE/FSE sequence with deep learning–based reconstruction demonstrated image quality comparable to that at 1.5T. Moreover, the 0.55T parameterisation was readily accommodated within the specific absorption rate (SAR) limits imposed by the HiRes 90K™ cochlear implant, whereas modifications required at 1.5T resulted in prolonged scan times and more noticeable participant motion artefact (Fig. 3).

Our finding of a similar proximity of hard artefact at 0.55T and 1.5T is consistent with the permanent internal magnetisation of the CI magnet likely being constant at both field strengths. Quantitative comparisons of artefact size have previously been performed only at 1.5T and 3T [23, 25, 26], where no consistent differences were demonstrated, although the MRI Safety Manual for the Advanced Bionics HiRes Ultra 3D cochlear implant reports a greater artefact radius at 3T compared to 1.5T [44]. Literature reports remain variable regarding the extent of artefact and the degree of anatomical obscuration associated with different T2-weighted temporal bone sequences [23, 45]. Some studies have reported that 2D T2-FSE sequences are associated with reduced artefactual obscuration of both ipsilateral and contralateral temporal bone structures compared with CISS imaging [27, 28, 45], whereas Kalmanson et al. quantified artefact extent and found it more extensive with 2D T2-FSE than CISS [23].

Several study limitations should be acknowledged. Firstly, the exploratory design and relatively small sample size limited the ability to perform robust statistical analyses or draw definitive conclusions. Secondly, methodological factors may have influenced the observed outcomes. Repeated magnet tilting could have induced fatigue within the silicone CI housing, and partial demagnetisation of the CI magnet during earlier MRI sessions may have altered its susceptibility to displacement in subsequent scans. Additionally, a practical trade-off existed between accurately assessing magnet position after the first scan and reapplying the head bandage in a precisely consistent position for subsequent imaging, which may have introduced variability. Thirdly, it should be acknowledged that the bandaging of an externally applied CI does not accurately mimic the anatomy of the implanted patient. For instance, CI magnet displacement or pain perception is unlikely to occur with the same frequency whilst an intracochlear electrode will influence inner ear visibility. The delineation of the electrode array in patients should be a focus of future studies since it will benefit from reduced local susceptibility artefact from the paramagnetic platinum electrode array at 0.55T and would benefit from 3D sequences. Finally, several aspects of the imaging analysis of CI artefact extent warrant consideration. Only two sequences were evaluated, and the extent to which these findings generalise to other temporal bone protocol, such as 3D-FSE or T1-weighted imaging, is therefore limited. Direct comparison of artefact between different implant types was not feasible, as devices were positioned at different locations. Moreover, even intra-individual comparisons between scanners may have been confounded by subtle variations in head positioning, including degrees of flexion [22]. There were also inherent differences in sequence design across field strengths. At 0.55 T, 2D T2-weighted imaging incorporated deep learning–based reconstruction and shorter acquisition times, whereas at 1.5 T the 2D T2-weighted sequence required adaptation for use with the HiRes 90K CI due to SAR constraints. The resulting longer acquisition time at 1.5 T contributed to motion artefact in some participants, further limiting comparability.

Conclusion

This exploratory study demonstrated reduced displacement of axial CI magnets but not rotating diametric magnets during 0.55T MRI as compared with 1.5T MRI, and this was consistent with objective measurements of lower magnetic forces acting on the implant. Participant-reported pressure perception did not differ between field strengths, and it is likely that the bandaging of the externally applied CI does not adequately mimic the pain sensation of an implanted device. Temporal bone T2w sequences adapted to reduce CI magnet artefact produced clinically acceptable imaging with good visibility of ipsilateral anatomical structures at 0.55T and with a similar extent of hard artefact to 1.5T. This study provides first evidence that lower field MRI may be a useful addition to the imaging of CIs, and particularly in those patients with axial magnet CIs who have experienced magnet complications or pain when undergoing high field MRI. Wider applicability to other auditory implants should be explored.

Declarations

1. ***Guarantor:***

The scientific guarantor of this publication is Dr Steve Connor

2. ***Ethical Approval and consent to participate :***

Institutional Review Board approval was obtained from the Health Faculties (Purple) Research Ethics Subcommittee.institutional ethics committee (Reference: HR/DP-23/24-40213). The research was conducted in accordance with the Declaration of Helsinki. Written informed consent was obtained from all participants in this study.

3. ***Availability of data and material***

The datasets used and/or analysed during the current study are available from the corresponding author on reasonable request.

4. ***Competing Interest:***

The authors of this manuscript declare no relationships with any companies, whose products or services may be related to the subject matter of the article.

5. ***Funding***

This research was funded by Rinri Therapeutics Ltd, and inactive cochlear implant models were provided by Advanced Bionics GmbH. The funder did not have any specific role in the conceptualization, design, data collection, analysis, decision to publish, or preparation of the manuscript. Authors also acknowledge funding support from Wellcome/Engineering and Physical Sciences Research Council Centre for Medical Engineering at King's College London (WT 203148/Z/16/Z); National Institute for Health Research Biomedical Research Centre at Guy's & St Thomas' Hospitals and King's College London; Cancer Research UK National Cancer Imaging Translational Accelerator (A27066); the UK Research & Innovation London Medical Imaging and Artificial Intelligence Centre.

6. ***Authors Contributions***

SC Conceptualised and designed the study/helped acquire and contributed to analysis of imaging data/conducted CI bandaging and pressure assessment scores/performed statistical analysis/wrote manuscript

AP helped acquire and provided advice on acquisition of imaging/acquired CI torque and longitudinal force data/contributed to manuscript and edited manuscript

IP Provided advice and training for bandaging CIs and recruiting participants

PT/CD Contributed to imaging analysis

PB/PD-C/LB Helped acquire imaging data

DW Helped acquire CI torque and longitudinal force data

OL Contributed to analysis of imaging data

SO Provided resources to conduct study and advised on scientific design

JH Primary support and advice for the design of the study and analysis of results/edited manuscript

All authors read and approved the final manuscript

Abbreviations

CI cochlear implant

CISS constructive interference in steady state

CPA cerebellopontine angle cistern

EAM external auditory meatus

FSE fast spin echo

IAM internal auditory meatus

ICC intraclass correlation coefficient

MRI magnetic resonance imaging

nM newton-metres

SAR specific absorption rate

T2w T2-weighted

T tesla

VAS visual analogue scale

References

1. Shen Y, Zhou T, Zou W, Zhang J, Yan S, Ye H, Huang W. Global, regional, and national burden of hearing loss from 1990 to 2021: findings from the 2021 global burden of disease study. Annals of Medicine. 2025; 57. https://doi.org/10.1080/07853890.2025.2527367
2. Zeng F-G. Celebrating the one millionth cochlear implant. JASA Express Lett.2022; 2, 077201 https://doi.org/10.1121/10.0012825

3. Martella M, Lenzi J, Gianino MM. Diagnostic technology: Trends of use and availability in a 10-year period (2011–2020) among Sixteen OECD Countries. Healthcare.2023; 11, 2078. https://doi.org/10.3390/ healthcare11142078
4. Magnetic Resonance Imaging (MRI) Equipment Market Size, Share & Industry Analysis, By Strength. https:// www.fortunebusinessinsights.com/industry-reports/magnetic-resonance-imaging-mri-equipment-market-100087.Accessed 22/3/26.
5. Kalin R, Stanton MS. Current clinical issues for MRI scanning of pacemaker and defibrillator patients. Pacing Clin Electrophysiol.2025; 28:326–8. https://doi.org/10.1111/j.1540-8159.2005.50024.x
6. Kim BG, Kim JW, Park JJ, Kim SH, Kim HN, Choi JY. Adverse events and discomfort during magnetic resonance imaging in cochlear implant recipients. JAMA Otolaryngol Head Neck Surg.2015;141:45-52. doi: 10.1001/jamaoto.2014.2926. PMID: 25411817.
7. Pross SE, Ward BK, Sharon JD, Weinreich HM, Aygun N, Francis HW. A Prospective study of pain from magnetic resonance imaging with cochlear implant magnets in situ. Otol Neurotol. 2018; 39:e80-e86. doi: 10.1097/MAO.0000000000001661. PMID: 29210950.
8. Shew M, Wichova H, Lin J, Ledbetter LN, Staecker H. Magnetic resonance imaging with cochlear implants and auditory brainstem implants: Are we truly practicing MRI safety? The Laryngoscope. 2019; 129: 482-489. https://doi.org/10.1002/lary.27516
9. Tam YC, Lee JWY, Gair J, Jackson C, Donnelly NP, Tysome JR, Axon PR, Bance ML. Performing MRI scans on cochlear Implant and auditory brainstem implant recipients: Review of 14.5 years' experience. Otol Neurotol. 2020;41:e556-e562. doi: 10.1097/MAO.0000000000002569. PMID: 31985706.
10. Bestourous DE, Davidson L, Reilly BK. A review of reported adverse events in MRI-Safe and MRI-Conditional cochlear implants. Otol Neurotol. 2022; 43 :2-47. doi: 10.1097/MAO.0000000000003339
11. Canzi P, Carlotto E, Zanoletti E, Frijns JHM, Borsetto D, Caruso A, Chiapparini L, Ciorba A, Conte G, Creber N et al. Multi-magnet cochlear implant technology and magnetic resonance imaging: The safety issue. Audiol. Res. 2024; 14, 401–411. https://doi.org/10.3390/audiolres14030034
12. Helbig S, Thiemann N, Hattingen E, Loth A, Stover T, Leinung M. Prospective study on magnetic resonance imaging in cochlear implant patients. Eur Arch Otorhinolaryngol, 2024; 281: 1231–1242. https://doi.org/10.1007/s00405-023-08224-1
13. Loth AG, Fischer K, Hey AK, Weiß R, Leinung M, Burck I, Linke A, Kramer S, Stöver T, Helbig S. Magnetic resonance imaging in patients with hearing implants – Follow-up on prevalence and complications. Otol Neurotol.2021; 42:1334-1341. doi:10.1097/MAO.0000000000003249
14. Patel EJ, Wu X, McLouth J, Sun DQ, Ward BK, Sharon JD. Pain, safety, and image quality of magnetic resonance imaging with cochlear implants: A prospective trial. Otolaryngol Head Neck Surg. 2025; 173: 705-712. https://doi.org/10.1002/ohn.1301
15. Todt I, Tittel A, Ernst A, Mittmann P, Mutze S. Pain free 3 T MRI scans in cochlear implantees. Otol Neurotol.2017; 38: e401-e404.doi:10.1097/MAO.0000000000001569
16. Todt I, Rademacher G, Grupe G, Stratmann A, Ernst A, Mutze S, Mittmann P. Cochlear implants and 1.5 T MRI scans: the effect of diametrically bipolar magnets and screw fixation on pain. J Otolaryngol Head Neck Surg. 2018; 47:11. doi: 10.1186/s40463-017-0252-9. PMID: 29402322; PMCID: PMC5799898.
17. Fierens G, Clemence M, Verhaert N, Bowtell R, Dewey R. The safety of active hearing implants in the ultra-high field magnetic resonance environment: A pilot study. Otol Neurotol. 2025; 46:1338-1345. doi: 10.1097/MAO.0000000000004638
18. Shellock FG. Radiofrequency energy-induced heating during MR procedures: a review. J Magn Reson Imaging. 2000; 12:30-6. doi: 10.1002/1522-2586(200007)12:1
19. Marques JP, Simonis FFJ, Webb AG. Low-field MRI: An MR physics perspective. J Magn Reson Imaging.2019; 49: 1528-1542. https://doi.org/10.1002/jmri.26637
20. Wiesmueller M, Kopp M, Sievert M et al. Comparison of vestibular schwannoma visualization between 0.55 T and 1.5 T MRI. Eur J Radiol. 2023; 165:110927. doi: 10.1016/j.ejrad.2023.110927. PMID: 37379624.
21. Dewey RS, Dineen RA, Clemence M, Dick O, Bowtell R, Kitterick P.Parametric assessment of the effect of cochlear implant positioning on brain MRI artefacts at 3 T. Otol Neurotol. 2021; 42: e1449-e1456. doi: 10.1097/MAO.0000000000003281
22. Ay N, Gehl HB, Sudhoff H, Todt I. Effect of head position on cochlear implant MRI artifact. Eur Arch Otorhinolaryngol. 2021; 278, 2763–2767. https://doi.org/10.1007/s00405-020-06349-1
23. Kalmanson OA, Talmage GD, Honce JM, Gubbels SP. Effect of head position and magnetic resonance sequence on cochlear implant-related artifact size and internal auditory canal visibility. Otol Neurotol. 2023; 44:e73-e80. doi:10.1097/MAO.0000000000003738. PMID: 36624593; PMCID: PMC10038139
24. Kim R, Schleyer S, Björn Gehl H, Sudhoff H, Goon P, Todt I. Intraindividual Comparison of Image Artifacts of Two Generations of Rotatable Cochlear Implant Magnets. J Int Adv Otol. 2024; 20:306-311. doi: 10.5152/iao.2024.231466. PMID: 39161162; PMCID: PMC11363200.
25. Majdani E, Majdani O, Steffens M, Warnecke A, Lesinski-Schiedat A, Lenarz T, Götz F. Dimensions of artefacts caused by cochlear and auditory brainstem implants in magnetic resonance imaging. Cochlear Implants International. 2020; 21:67–74. https://doi.org/10.1080/14670100.2019.1668617.
26. Todt I, Guerkov R, Gehl HB, Sudhoff H. Comparison of cochlear implant magnets and their MRI artifact size. Biomed Res Int. 2020; 10 :5086291. doi: 10.1155/2020/5086291. PMID: 32420348; PMCID: PMC7199598
27. Tysome JR, Tam YC, Patterson I, Graves MJ, Gazibegovic D. Assessment of a novel 3T MRI compatible cochlear implant magnet: Torque, forces, demagnetization, and imaging. Otol Neurotol. 2019.40: e966-e974. doi: 10.1097/MAO.0000000000002407
28. Winchester A, Kay-Rivest E, Bruno M, Hagiwara M, Moonis G, Jethanamest D. Image quality and artifact reduction of a cochlear implant with rotatable magnets. Otol Neurotol. 2023; 44: e223-e229. doi: 10.1097/MAO.0000000000003840
29. ASTM International. ASTM F2052-21, standard test method for measurement of magnetically induced displacement force on medical devices in the magnetic resonance environment. 2021. doi:10.1520/F2052-21

30. ASTM International. ASTM F2213-17, standard test method for measurement of magnetically induced torque on medical devices in the magnetic resonance environment. 2017. doi: 10.1520/F2213-17
31. Breivik EK, Björnsson GA, Skovlund E. A comparison of pain rating scales by sampling from clinical trial data. Clin J Pain. 2000; 16:22-8. doi: 10.1097/00002508-200003000-00005. PMID: 10741815.
32. Horos Project. Horos™—Free, open-source DICOM viewer. Available at: http://www.horosproject.org).
33. Lin A, Menta AK, Ahmad SA, Zhang A, Perdomo D, Reddy A, Ward BK. A comprehensive analysis of MRI-related cochlear implant adverse events reported by FDA's manufacturer and user facility device experience database. Laryngoscope Investigative Otolaryngology. 2025; 10: e70073. doi:10.1002/lio2.70073
34. Young NM, Rojas C, Deng J, Burrowes D, Ryan M. Magnetic resonance imaging of cochlear implant recipients. Otol Neurotol. 2016; 37:665-671. doi: 10.1097/mao.0000000000001053. PMID: 27153331.
35. Grupe G, Wagner J, Hofmann S, Stratmann A, Mittmann P, Ernst A, Todt I. Prevalence and complications of MRI scans of cochlear implant patients HNO. 2017. 65(Suppl 1):35-40. doi: 10.1007/s00106-016-0129-7. PMID: 26886493.
36. Smith ME, Daniel J. Moualed DJ, Freeman SR, Stapleton EJ, Anup R, Kurian J, Jarvis N, Thomas OM, Lloyd SKW. The experience of auditory implant recipients undergoing magnetic resonance imaging: Factors associated with pain, Cochlear Implants International. 2023; 24:5, 260-267, DOI: 10.1080/14670100.2023.2172828
37. Gubbels SP, McMenomey SO. Safety study of the Cochlear Nucleus® 24 device with internal magnet in the 1.5 Tesla magnetic resonance imaging scanner. The Laryngoscope. 2006; 116: 865-871. https://doi.org/10.1097/01.MLG.0000216807.03225.CE
38. Johnson BJ, Macielak RJ, Watson RE, Heimer JM, Wiste BJ, Lane JI, Edmonson HA, Carlson ML. Magnetic resonance imaging in patients with cochlear implants without magnet removal: A radiology-administered protocol to enhance operational efficiency and improve workflow. Otol Neurotol. 2003; 44:664-671. doi: 10.1097/MAO.0000000000003898.
39. Weber BP, Goldring JE, Santogrossi T, Koestler H, Tziviskos G, Battmer R, Lenarz Th. Magnetic resonance imaging compatibility testing of the Clarion 1.2 cochlear implant. Am J Otol. 1998; 19 :584-90. PMID: 9752965.
40. Rupp R, Balk M, Sievert M, Leibl V, Schleder S, Allner M, Iro H, Hoppe U, Hornung J, Gostian AO. Risk of magnetic resonance imaging-induced magnet dislocation for different types of cochlear implants: a single-center retrospective study. J Otolaryngol Head Neck Surg. 2023; 52 :28. doi: 10.1186/s40463-023-00633-w. PMID: 37085925; PMCID: PMC10122328.
41. Jensen K, Andersen HO; Olesen J, Lindblom U. Pressure-pain threshold in human temporal region. Evaluation of a new pressure algometer. Pain. 1986; 25:313-323. doi: 10.1016/0304-3959(86)90235-6
42. Youssefzadeh S, Baumgartner W, Dorffner R, Gstöttner W, Trattnig S. MR Compatibility of Med EL Cochlear Implants: Clinical Testing at 1.0 T. Journal of Computer Assisted Tomography. 1998; 22:346-350.ndoi: 10.1097/00004728-199805000-00002.
43. Stratmann A, Mittmann P, Rademacher G, Grupe G, Hoffmann S, Mutze S, Ernst A, Todt I. MRI-based estimation of scalar cochlear-implant electrode position. Biomed Res Int. 2017; 2017:6372704. doi: 10.1155/2017/6372704. PMID: 29181399; PMCID: PMC5664259.
44. HiRes™ Ultra 3D MRI Safety Information. https://www.advancedbionics.com/content/dam/advancedbionics/documents/libraries/mri-safety/hires-ultra-3d-mri-safety-information.pdf
45. Wagner F, Wimmer W, Leidolt L, Vischer M, Weder S, Wiest R, Mantokoudis G, Caversaccio MD et al. Significant artifact reduction at 1.5T and 3T MRI by the Use of a cochlear implant with removable magnet: An experimental human cadaver study. PLoS ONE. 2015; 10: e0132483. doi: 10.1371/journal.pone.0132483

Tables

Table 1: Demographic, location of CI bandaging and order of the MRI scanning

	Age/sex	Laterality	Nasion-EAM angle (degrees)	Distance from EAM (cm)	Order of scans
1	32F	R	120	8	0.55T/1.5T
2	51F	R	120	8	1.5T/0.55T
3	33M	L	135	8	0.55T/1.5T
4	40M	R	150	9	0.55T/1.5T
5	53F	R	90	9	1.5T/0.55T
6	31M	L	120	10	1.5T/0.55T
7	37M	L	120	8	1.5T/0.55T
8	55F	L	90	9	0.55T/1.5T
9	29M	R	150	9	1.5T/0.55T
10	37M	R	135	9	0.55T/1.5T

Table 2: Pressure sensation (VAS) scores with 1.5T and 0.55T scanning for the HiRes™

Ultra 3D and HiRes™ 90K CI magnets

		1.5T			0.55T		
Participant	**Type of CI**	**Pressure score increases when entering bore**	**Pressure scores increase during scanning**	**Magnet displacement after MRI (tilted/dislocated)**	**Pressure score increases when entering bore**	**Pressure scores increase during scanning**	**Magnet displacement after MRI (tilted/dislocated)**
1	HiRes™ Ultra 3D	1	2	N	0	0	N[a]
2	HiRes™ Ultra 3D	0	2	N	0	1	N[a]
3	HiRes™ Ultra 3D	0	0	N[a]	0	0	N
4	HiRes™ Ultra 3D	0	0	N	1	2	N[a]
5	HiRes™ Ultra 3D	0	0	N	0	0	N
6	HiRes™ 90K	1	2	Y dislocated	0	2	N
7	HiRes™ 90K	0[c]	1	Y tilted	0	1	N
8	HiRes™ 90K	0[c]	3	Y tilted	2	6[b]	N
9	HiRes™ 90K	0	6[b]	Y dislocated	0	1	N
10	HiRes™ 90K	0	3	N	0	4	N

a The magnet was not inspected after the first MRI scan session but was undisplaced after both sessions were completed

b The scores of 6 in these patients were short-lived and the participant felt it may have been due to direct pressure from the head coil on the bandaged CI

c Sensation of clicking when entering scanner bore

Table 3: Qualitative scoring of image quality, diagnostic confidence and cochlear implant artefact obscuration

Score	Image quality	Diagnostic confidence	Reduced visualisation due to cochlear implant related artefact	Second stage direct comparison of 1.5T v 0.55T
0	Very low	Very low: Poor visibility of entire structure	None of the structure is visualised due to CI related artefact	Much better image quality/greater diagnostic confidence/less artefact with case A
1	Low	Low: Significantly reduced visualisation of structure or poorly defined	Minority of structure visualised due to CI related artefact	Better image quality/greater diagnostic confidence/less artefact with case A
2	Medium/Adequate	Medium: Moderately reduced but adequate visualisation and definition of structure	Majority of structure visualised due to CI related artefact	Equal image quality/greater diagnostic confidence/less artefact with case A and B
3	Good	Good: Minor reduction in visualisation or definition of structure	Visualised entirely with minor artefact due to CI related artefact	Better image quality/greater diagnostic confidence/less artefact with case B
4	Very good	Very good: Entirely visualized and well-defined structure without any artefact	Visualised entirely and no hard/soft artefact extension to structure (distortion or obscuration) due to CI related artefact	Much better image quality/greater diagnostic confidence/less artefact with case B
Guidance	Assessed away from artefact within the anterior image	Allows for cochlear implant related or another artefact. Based on visibility and clarity of cranial nerves and depiction of fluid containing structures	Assesses soft or hard artefact related to the cochlear implant	The second stage comparison was blinded to the MRI field strength, and scoring was again performed across image quality, diagnostic confidence and cochlear implant artefact obscuration themes

Table 4: Qualitative evaluation of image quality, diagnostic confidence and visualisation without cochlear implant related artefact for ipsilateral and contralateral anatomical sites: Differences in scores between sequences and MRI field strengths and inter-rater correlation coefficients

		0.55T: CISS v T2 2D FSE		1.5T: CISS v T2 2D FSE		CISS: 1.5 v 0.55T		T2 2D FSE: 1.5 v 0.55T	
	ICC (95% CI)	Median and Superior rankings	p value effect size[a] (r)	Median and Superior rankings	p value effect size[a] (r)	Median and Superior rankings (second scoring)[b]	p value effect size[a] (r)	Median and Superior rankings (second scoring)[b]	p value effect size[a] (r)
Image quality	0.52 (0.10-0.76)	3/3	1.00	4/3	0.27	4/3	0.25	3/3	1.00
		2/2	0	4/2	0.38	3/0 (4/0)	**0.65**	2/2 (2/2)	0
CI side									
Diagnostic confidence									
CPA	0.64 (0.07-0.85)	2/2	0.50	3/2	1.00	3/2	0.19	2/2	0.19
		3/1	0.43	3/1	0.14	5/1 (4/0)	**0.63**	2/1(1/1)	0.14
IAM	0.65 (0.23-0.84)	2/3	0.38	3/3	0.75	3/2	0.06	3/3	0.75
		1/3	0.49	2/3	0.27	5/1(5/1)	**0.80**	2/1(1/1)	0.27
Inner ear	0.84 (0.67-0.92)	2/4	0.06	3/4	0.25	3/3	0.50	4/4	1.00
		0/5	**0.78**	1/3	**0.58**	3/1(3/0)	0.43	1/2(1/2)	0
Visualisation without CI related artefact									
CPA	0.85 (0.71-0.92)	3/4	**0.02**	3/4	**0.02**	3/3	1.00	4/4	1.00
		0/7	**0.93**	0/7	**0.93**	2/1(3/2)	0.38	1/0(0/0)	0.38
IAM	0.78 (0.58-0.89)	2/4	**0.02**	¾	0.25	3/3	0.76	4/4	1.00
		0/7	**1.00**	0/3	**0.62**	2/1(3/1)	0.31	2/1(0/0)	0.22
Inner ear	0.92 (0.85-0.96)	2/4	**0.02**	3/4	0.13	3/2	0.18	4/4	1.00
		0/7	**0.93**	0/4	**0.70**	5/2(4/1)	0.48	2/1(2/2)	0.22
Contralateral side									
Diagnostic confidence									
CPA	0.62 (0.11-0.83)	3/2	0.38	4/3	0.16	3/2	0.38	3/2	0.38
		4/1	**0.51**	5/1	**0.65**	3/1(3/0)	**0.51**	3/1(2/1)	**0.51**
IAM	0.53 (0.16-0.76)	3/3	1.00	4/3	0.38	4/3	0.06	3/3	1.00
		1/2	0	4/1	**0.51**	5/0(3/0)	**0.80**	3/2(1/1)	0.17

Inner ear	0.51 (0.10-0.74)	¾	0.50	4/3	1.00	4/3	0.25	4/3	0.6
		0/2	**0.53**	4/3	0.14	2/0(2/0)	**0.53**	3/1(1/1)	0.38
Visualisation without CI related artefact									
CPA	0.87 (0.75-0.94)	4/4	0.25	4/4	0.50	4/4	1.00	4/4	1.00
		0/3	**0.65**	0/1	0.38	0/0(2/1)	0	0/0(0/0)	0
IAM	0.88 (0.77-0.94)	4/4	0.25	4/4	0.50	4/4	0.63	4/4	1.00
		0/3	**0.65**	0/1	0.38	3/1(3/1)	0.38	0/0(0/0)	0
Inner ear	0.83 (0.67-0.91)	4/4	0.25	4/4	0.25	4/4	0.63	4/4	1.00
		0/3	**0.65**	0/3	**0.65**	3/1(3/1)	0.38	0/0(0/0)	0

[a] This refers to the effect size (r = Z/√n) of the sequence or field strength with the higher rankings

[b] The second scoring involved direct comparisons of the corresponding 1.5T and 0.55T sequences and was performed as a sensitivity analysis for the blinded scoring of the individual sequences so should be similar to the superior rankings

p values<0.05 and effect size > 0.5 are in bold

Table 5: Distances (cm) between hard artefact and anatomical structures: Mean differences between 0.55T with 1.5T with each sequence

	CISS						2D T2w-FSE				
	1.5t v 0.55T						1.5 T v 0.55T 2D T2w-FSE				
	number	Mean (SD) 1.5T	Mean (SD) 0.55T	Mean Difference (SD)	LOA lower (CIs)	LOA upper (CIs)	number	Mean (SD) 1.5T	Mean (SD) 0.55T	Mean Difference (SD)	LOA l (CIs)
Ipsilateral											
Axial											
Porus	6	1.86 (0.98)	2.42(1.55)	-0.56 (1.39)	-3.28 (-5.18/-1.38)	2.16 (0.26/4.06)	4	2.61(0.54)	2.86(1.42)	-0.25 (1.20)	-2.60 (-4.61
Cochlear aperture	6	2.00(0.96)	2.52(1.18)	-0.52 (1.14)	-2.74 (-4.29/-1.19)	1.71 (0.16/3.26)	4	3.01(0.57)	3.33(1.40)	-0.32 (1.25)	-2.77 (-4.86
Coronal											
Porus acousticus	7	1.59(0.89)	2.25(1.23)	-0.67 (1.28)	-3.17 (-4.79/-1.55)	1.84 (0.22/3.46)	3	2.61(0.73)	1.73(0.65)	+0.88 (0.48)	-0.06 (-0.99
Cochlear aperture	7	2.06(1.88)	2.23(1.06)	-0.17 (2.17)	-4.42 (-7.17/-1.97)	4.08 (1.33/6.83)	3	2.56(0.53)	1.89(0.81)	+0.67 (0.34)	0.01 (-0.65
Contralateral side											
Axial											
Porus acousticus	6	5.93(1.35)	6.64(2.19)	-0.71 (1.76)	-4.16 (-6.57/-1.75)	2.75 (0.34-5.16)	4	6.59(0.88)	5.83(1.01)	+0.77 (0.23)	0.32 (-0.07
Cochlear aperture	6	6.87(1.36)	7.47(2.25)	-0.60 (1.75)	-4.03 (-6.42/-1.64)	2.83 (0.44/5.22)	4	7.37(0.96)	6.62(1.20)	+0.76 (0.35)	0.08 (-0.51

Table 6: Distances (cm) between hard artefact and anatomical structures: Mean differences between CISS and 2D T2-FSE with each field strength

	0.55T CISS V 2D T2w-FSE						1.5 T CISS V 2D T2w-FSE				
	number	Mean (SD) 1.5T	Mean (SD) 0.55T	Mean Difference (SD)	LOA lower (CIs)	LOA upper (CIs)	number	Mean (SD) 1.5T	Mean (SD) 0.55T	Mean Difference (SD)	LOA (CIs)
Ipsilateral											
Axial											
Porus acousticus	5	1.87 (0.84)	2.79(1.24)	-0.92 (1.15)	-3.17 (-4.89/-1.45)	1.33 (-0.39/3.05)	5	2.03(0.99)	2.88(0.75)	-0.85 (0.93)	-2.67 (-4.0
Cochlear aperture	5	2.17(0.91)	3.10(1.32)	-0.93 (1.06)	-3.01 (-4.6/-1.42)	1.15 (-0.44/2.74)	5	2.25(0.82)	3.04(0.50)	-0.79 (0.85)	-2.45 (-3.7
Coronal											
Porus	4	2.25(1.23)	2.03(0.80)	-0.25 (1.41)	-3.01 (-5.37/-0.65)	2.51 (0.15/4.87)	4	1.58(0.97)	2.61(0.72)	-1.03 (1.43)	-3.83 (-6.2
Cochlear aperture	4	1.88(1.23)	2.38(1.18)	-0.50 (1.98)	-4.39 (-7.71/-1.07)	3.39 (0.07/6.71)	4	2.69(2.29)	2.64(0.46)	0.054 (2.16)	-4.19 (-7.8
Contralateral side											
Axial											
Porus acousticus	5	5.86(1.21)	6.10(1.07)	-0.24 (0.91)	-2.02 (-3.38/-0.66)	1.54 (0.18/2.9)	5	5.87(1.49)	7.05(1.27)	-1.18 (1.11)	-3.36 (-5.3
Cochlear aperture	5	6.67(1.20)	6.86(1.17)	-0.20 (0.86	-1.89 (-3.18/-0.6)	1.48 (0.19/2.77)	5	7.06(1.35)	7.97(1.56)	-1.12 (1.14)	-3.35 (-5.0

Figures

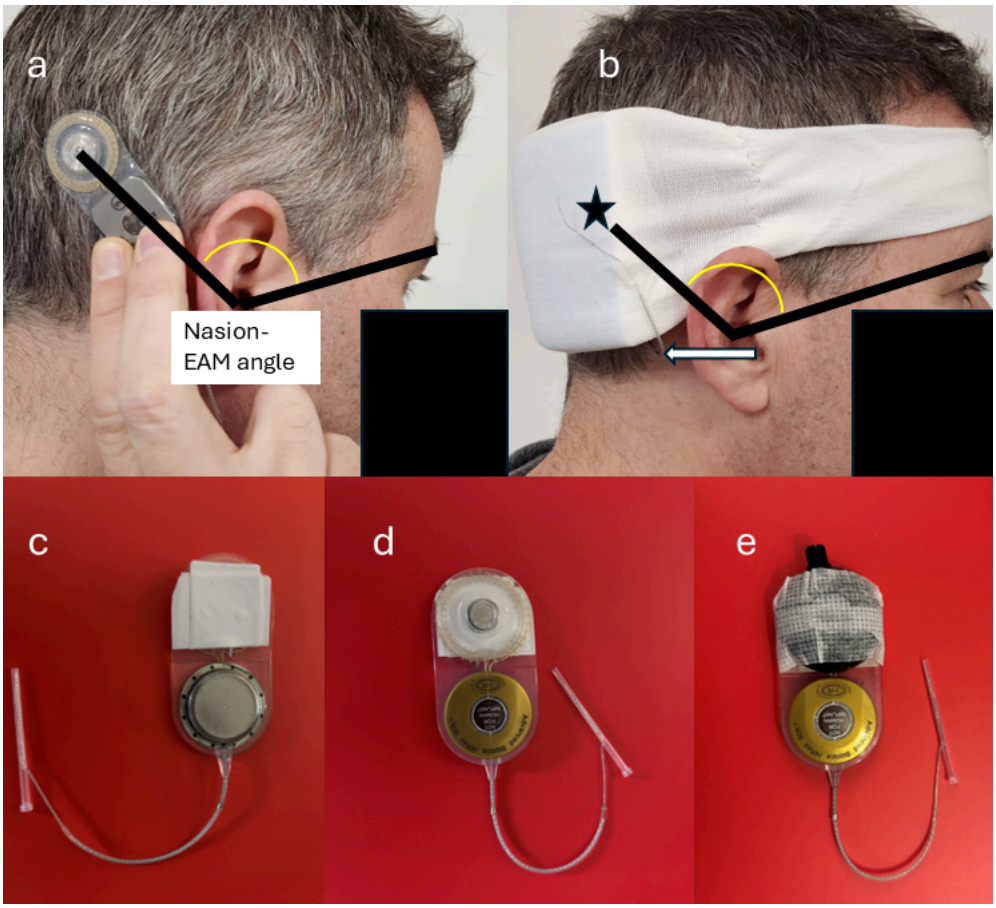


Figure 1

The positioning and bandaging of the CI and reinforcement of the CI magnet prior to MRI scanning. a) The CI is positioned at the designated nasion-EAM angle. A dummy processor was applied (removed in the image) to guide the appropriate distance from the EAM which was then recorded. b) The CI is bandaged with the electrode array (arrow) taped to the superficial aspect of the bandage. c) and d) Padding was applied to the deep aspect of the magnet silicone housing and e) a plastic disc was taped to the superficial aspect of the magnet housing.

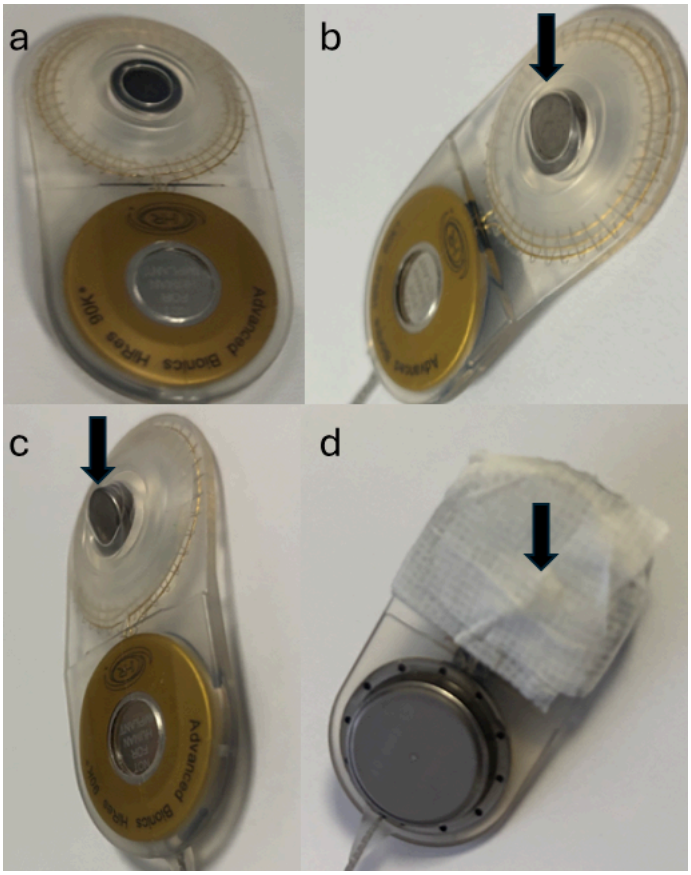


Figure 2

The evaluation of CI magnet displacement (HiRes 90K™ CI in the figure) after MRI scanning. a) Participant 8: The CI magnet after 0.55T MRI remains displaced within the magnet housing. b) Participant 8: The CI magnet after 1.5T MRI is tilted within the magnet housing but remains contained by the lip (arrow). c) and d) Participant 9: The CI magnet after 1.5T is dislocated from the magnet housing and is no longer contained by the lip (arrow in c) whilst on the underside of the magnet casing there is visible indentation of the padding (arrow in d).

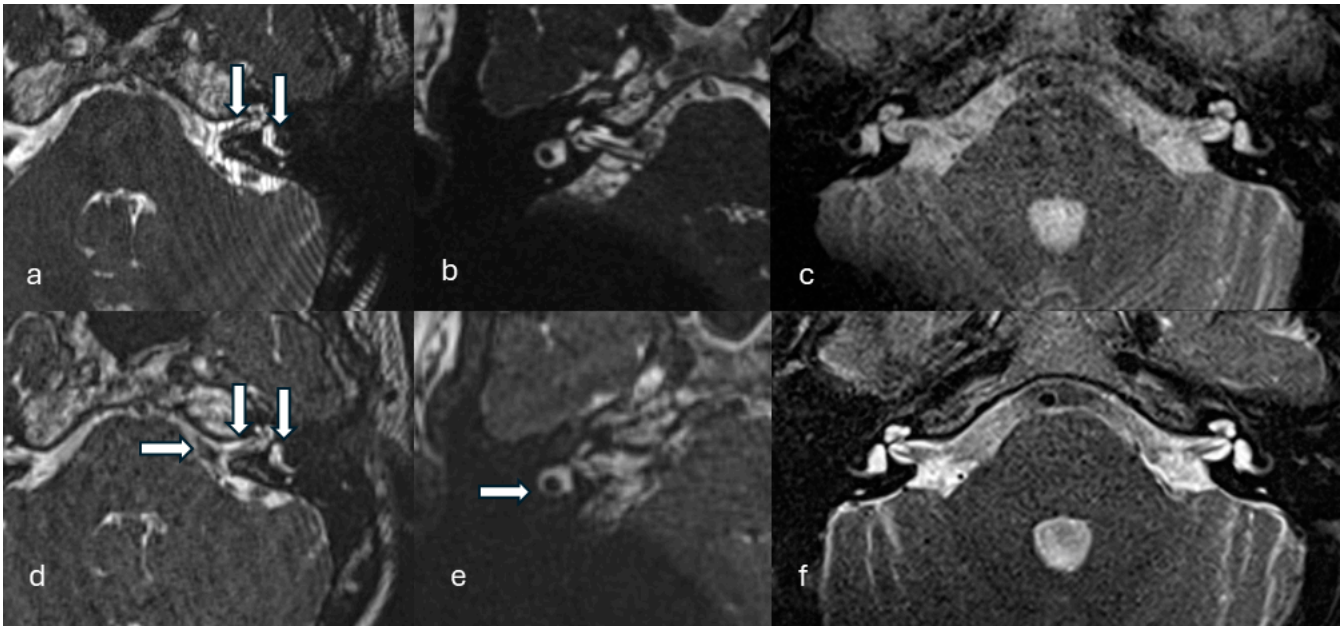


Figure 3

Paired temporal bone images at 0.55T and 1.5T illustrating the qualitative evaluation. a) 1.5T CISS image shows greater banding artefact (vertical arrows) across the CPA, IAM and inner ear than the corresponding d) 0.55T CISS image, whilst there is greater CSF flow related in the CPA on the 0.55T study artefact (horizontal arrow in d). Median scores for the IAM indicated high diagnostic confidence (score 4) and the majority of the structure being visualised without CI

related artefact (score 2) at 1.5T, whilst there were very high diagnostic confidence (score 4) and visualisation entirely without artefact (score 4) at 0.55T. Although there was no CI related artefact obscuring the CPA at 0.55T, the CSF flow artefact lowered the diagnostic confidence to adequate (score 2). b) 1.5T CISS image shows no CI related artefact obscuration of the lateral semicircular canal whilst there is obscuration on the e) 0.55T CISS image (arrow in e). Median scores for the inner ear indicated very high diagnostic confidence (score 4) and complete visualisation without artefact (score 4) at 1.5T whilst there was only adequate diagnostic confidence (score 2) reduced visualisation without CI related artefact (score 2) at 0.55T. c) 1.5T 2D T2-FSE and e) 0.55T 2D T2-FSE images demonstrate degradation of the 1.5T images. This resulted from participant motion during a prolonged scan due to the SAR limits imposed by the HiRes 90K™ cochlear implant. Whilst there is no CI related artefact, the blurring of the neural structures resulted in diagnostic confidence median scores for the left IAM of adequate (score 3) at 1.5T whilst it was high (score 4) at 0.55T.

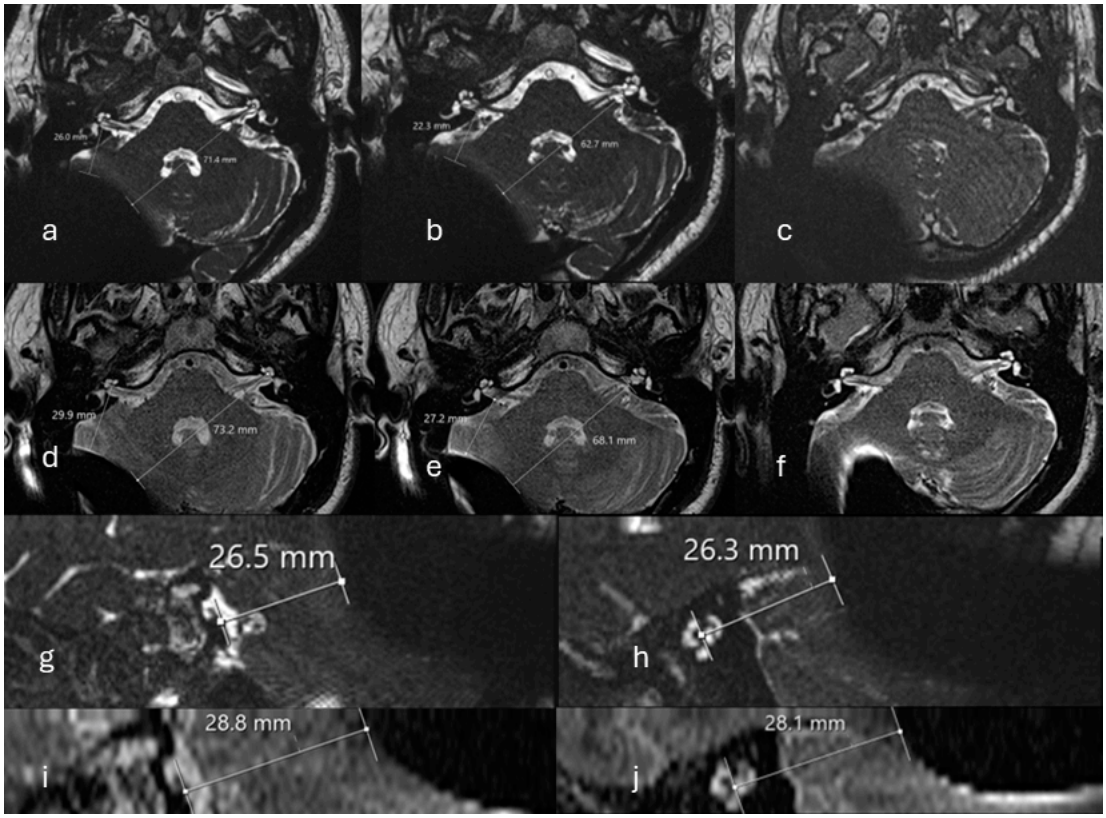


Figure 4

Measurement of the shortest distances between anatomical structures and the border of hard artefact. a) 1.5T CISS and d) 1.5T 2D T2-FSE demonstrate measurements to the ipsilateral and contralateral porus acousticus. b) 1.5T CISS and e) 1.5T 2D T2-FSE demonstrate measurements to the ipsilateral and contralateral cochlear aperture. The corresponding c) 0.55T CISS and f) 0.55T 2D T2-FSE images are shown. g) 1.5T CISS and i) 1.5T 2D T2-FSE demonstrate sagittal reformats and measurements to the ipsilateral porus acousticus, whilst h) 1.5T CISS and j) 1.5T 2D T2-FSE demonstrate measurements to the contralateral porus acousticus. Note the greater craniocaudal coverage of the CISS sequence; however, in all cases the nearest margin of hard artefact was confirmed to lie within the imaged volume on both sequences.

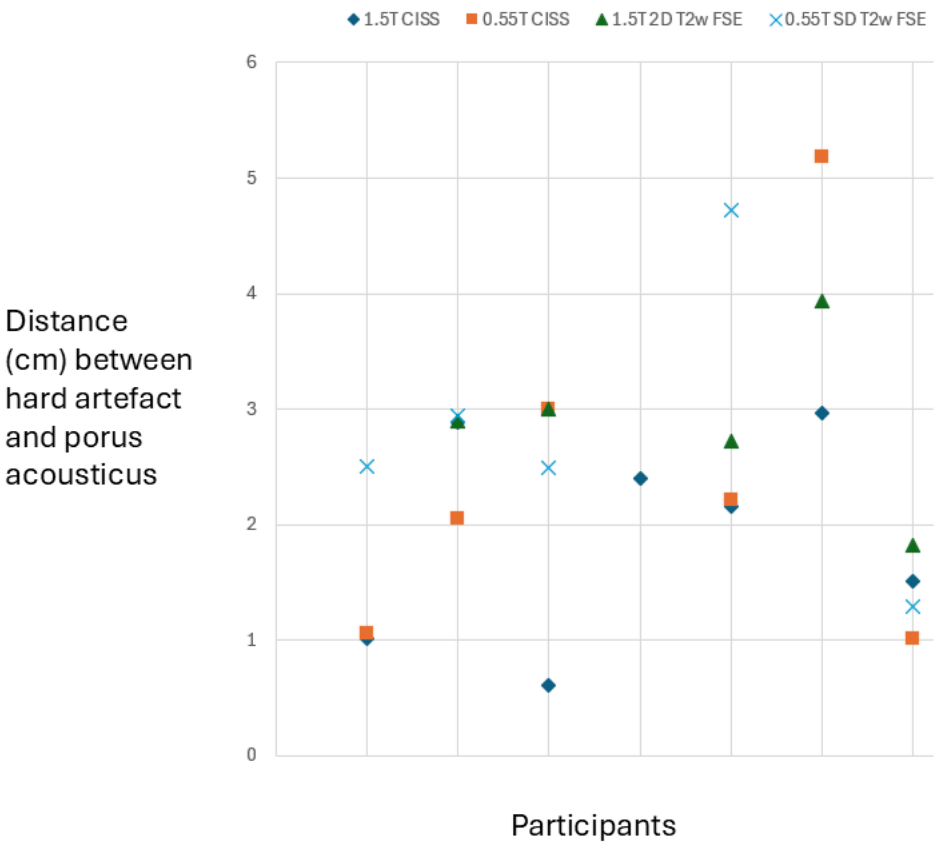


Figure 5

A plot of the distances between the nearest edge of the hard artefact and the porus acousticus for the 1.5T CISS, 0.55T CISS, 1.5T 2D T2-FSE and 0.55T 2D T2-FSE MRI studies for each of the participants. There was substantial interparticipant variability in the relative magnitude of distances between sequences.

Supplementary Files

This is a list of supplementary files associated with this preprint. Click to download.

- Supplementaryfigure1.pdf
- Supplementaryfigure2.pdf
- Supplementarytable1.docx
- Supplementarytable2.docx
- Supplementarytable3.docx